Dome of magnetic order inside the nematic phase of sulfur-substituted FeSe under pressure

Li Xiang,[1,2,*] Udhara S. Kaluarachchi,[1,2] Anna E. Böhmer,[1] Valentin Taufour,[1,3] Makariy A. Tanatar,[1,2]
Ruslan Prozorov,[1,2] Sergey L. Bud'ko,[1,2] and Paul C. Canfield[1,2]

[1]*Ames Laboratory, Iowa State University, Ames, Iowa 50011, USA*
[2]*Department of Physics and Astronomy, Iowa State University, Ames, Iowa 50011, USA*
[3]*Department of Physics, University of California, Davis, California 95616, USA*

The pressure dependence of the structural, magnetic, and superconducting transitions and of the superconducting upper critical field were studied in sulfur-substituted $Fe(Se_{1-x}S_x)$. Resistance measurements were performed on single crystals with three substitution levels ($x = 0.043, 0.096, 0.12$) under hydrostatic pressures up to 1.8 GPa and in magnetic fields up to 9 T and were compared to data on pure FeSe. Our results illustrate the effects of chemical and physical pressure on $Fe(Se_{1-x}S_x)$. On increasing sulfur content, magnetic order in the low-pressure range is strongly suppressed to a small domelike region in the phase diagrams. However, T_s is much less suppressed by sulfur substitution, and T_c of $Fe(Se_{1-x}S_x)$ exhibits similar nonmonotonic pressure dependence with a local maximum and a local minimum present in the low-pressure range for all x. The local maximum in T_c coincides with the emergence of the magnetic order above T_c. At this pressure the slope of the upper critical field decreases abruptly, which may indicate a Fermi-surface reconstruction. The minimum of T_c correlates with a broad maximum of the upper critical field slope normalized by T_c.

I. INTRODUCTION

Despite a large number of different compounds, many iron-based superconductors share similar physical properties. A characteristic feature of this material class is rich phase diagrams, containing an antiferromagnetic phase, which is suppressed upon substitution or pressure, and superconductivity, which emerges at a critical value of this tuning parameter [1,2]. Usually, the antiferromagnetic ordering is of the stripe type and is preceded or accompanied by a structural tetragonal-to-orthorhombic distortion, associated with electronic nematic order [3]. The magnetic and structural transitions typically extrapolate to zero temperature near the maximum of the superconducting T_c dome, suggesting the possibility that magnetic or nematic fluctuations surrounding a quantum critical point mediate superconductivity [4,5].

Among all the iron-based superconductors, the structurally simplest binary compound, FeSe, does not share this common behavior. First, the structural and magnetic transitions are well separated [6]; at ambient pressure, a tetragonal-to-orthorhombic structural transition occurs at $T_s = 90$ K. The low-temperature phase has been identified as nematic due to the similarity of this transition to the structural transition typical of many iron-based superconductors [6–9]. However, there is no signature of magnetic order observed at ambient pressure down to 0.24 K [10]. Very recent specific-heat data indicate a possible antiferromagnetic transition at 1.08 K [11]. However, these results contradict previous results [12], in which no anomaly in the specific measurement near this temperature was observed.

Second, under approximately 0.8 GPa of applied pressure, magnetic order clearly emerges [10,13–15] above T_c, and the magnetic transition temperature T_m exhibits a domelike pressure dependence between 0.8 and 6 GPa [16,17]. Strong coupling between orthorhombic distortion and magnetic order

under pressure was demonstrated [18]. Nevertheless, the large separation of T_s and T_m at ambient pressure raises the question of how the nematic order and magnetism are related in this compound [19–22].

Third, the pressure dependence of the superconducting transition temperature T_c shows a remarkable nonmonotonic structure, with a local maximum of T_c around 0.8 GPa, a local minimum around 1.2 GPa, a plateau around 4 GPa, and, finally, a maximum of 37 K around 6 GPa, before T_c decreases at even higher pressures [15,16,23]. Moreover, recent studies found that monolayer thin films of FeSe on $SrTiO_3$ show superconducting behavior at temperatures higher than 100 K [24]. Hence, FeSe gives us a unique opportunity to study how nematicity, magnetism and superconductivity interact with each other.

The maximum T_c of bulk FeSe under pressure is achieved in the pressure range above 5 GPa. However, FeSe has a complex and interesting phase interplay in the pressure range below 2 GPa. The intersection of the nematic phase, magnetic order, and superconductivity falls in this pressure range [14–16]. Several studies have investigated the effect of sulfur substitution on FeSe [25–29]. Similar to applied pressure, sulfur substitution suppresses T_s. In contrast to pressurized FeSe, no magnetic ordering is found in the substitution-temperature phase diagram of $Fe(Se_{1-x}S_x)$, and T_c is only moderately enhanced to 11 K by substitution [26]. In this work, we combine chemical pressure through sulfur substitution up to 12% and physical pressure up to 1.8 GPa and show that the pressure-induced magnetic phase is strongly suppressed upon substitution in this pressure range. In contrast, the nematic phase and superconducting phase are quite robust, and their behaviors under pressure do not change qualitatively.

II. EXPERIMENTAL DETAILS

High-quality single crystals of $FeSe_{1-x}S_x$ [$x = 0.043(5)$, $x = 0.096(1)$, $x = 0.12(2)$] with sharp superconducting
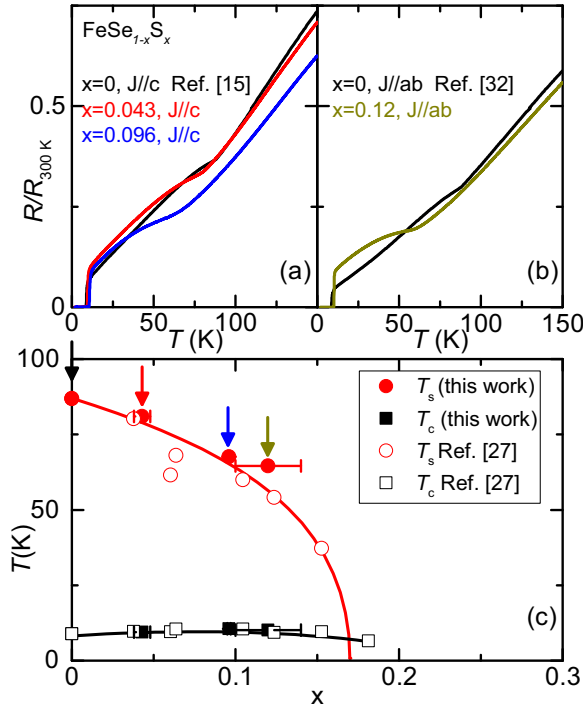
*ives@iastate.edu

FIG. 1. (a) Temperature dependence of the normalized resistance of Fe(Se$_{1-x}$S$_x$) single crystals with current applied along the c axis for $x = 0$, $x = 0.043$, and $x = 0.096$. The data on the parent compound FeSe are taken from Ref. [15]. (b) Temperature dependence of the normalized resistance of Fe(Se$_{1-x}$S$_x$) single crystals with current applied in the ab plane for $x = 0$ and $x = 0.12$. The data on the parent compound FeSe are taken from Ref. [32]. (c) Substitution-temperature phase diagram of Fe(Se$_{1-x}$S$_x$). The four compounds we used in this work are marked. Open symbols are data taken from Ref. [27].

transitions at ambient pressure [see Figs. 1(b)–5(b)] were grown using chemical vapor transport, similar to the process in Ref. [30]. The substitution level x was determined by energy-dispersive x-ray spectroscopy (EDS), and the given values and errors correspond to the average and standard deviation of EDS results obtained on about ten spots from, typically, three different samples per batch, respectively. The c-axis resistance was measured on samples with substitution levels $x = 0.043$ and 0.096 with approximate dimensions of $(0.5 \times 0.5 \times 0.1)$ mm^3, using a two-probe technique similar to that in Refs. [15,31]. Two Ag wires were attached to the samples by soldering with an In-Ag alloy [15,32]. The contact resistance is less than $50\,\mu\Omega$, which is much smaller than the sample resistance of approximately 10 mΩ. Four-probe wiring was used down to the sample contacts. The in-plane resistance was measured on a sample with a substitution level $x = 0.12$ with approximate dimensions of $(1 \times 0.5 \times 0.1)$ mm^3 in a standard four-contact configuration, with contacts prepared using silver epoxy. The ac resistance measurement was performed in a Quantum Design Physical Property Measurement System using 1-mA, 17-Hz excitation, on cooling and warming at a rate of 0.25 K/min. A Be-Cu/Ni-Cr-Al hybrid piston-cylinder cell similar to the one described in Ref. [33] was used to apply pressure. Pressure values at low
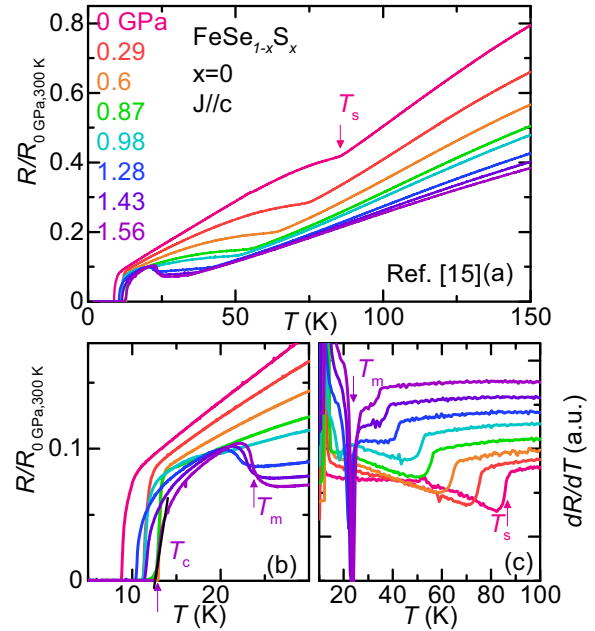

FIG. 2. (a) Evolution of the c-axis resistance with hydrostatic pressure for pure FeSe. Data were normalized at room temperature and ambient pressure. (b) Blowup of the low-temperature region. (c) Temperature derivative dR/dT showing the evolution of structural transition T_s. Data are taken from Ref. [15]. Examples of transition temperatures T_s, T_m, and T_c are indicated by arrows.

temperature were inferred from the $T_c(p)$ of lead [34]. Good hydrostatic conditions were achieved by using a 4:6 mixture of light mineral oil:n-pentane as the pressure medium, which solidifies at room temperature in the range 3–4 GPa, i.e., well above our maximum pressure [33,35,36].

III. PRESSURE-TEMPERATURE PHASE DIAGRAMS

Figure 1 shows the ambient-pressure resistance of the studied Fe(Se$_{1-x}$S$_x$) samples. The resistance is normalized at 300 K. The c-axis and in-plane resistance data on the parent compound FeSe are taken from Refs. [15,32], respectively. T_c increases slightly from 8.9 K for undoped FeSe to 10.1 K for $x = 0.12$. The structural transition, visible as a kink in the resistance data, is suppressed from 90 to 60 K at the highest studied substitution level. Note that in this work, the in-plane resistance is studied for the $x = 0.12$ sample, but c-axis resistance is studied for the other three substitution levels. The features at T_s in in-plane and interplane resistance are rather similar. The positions of the studied compositions are indicated in the composition-temperature phase diagram in Fig. 1(c).

Figures 2(a)–5(a) show the pressure dependence of the resistance of Fe(Se$_{1-x}$S$_x$) for $x = 0$, $x = 0.043$, 0.096, and 0.12, respectively. In these plots the resistance is normalized by dividing it by the ambient-pressure, room-temperature value for each sample. In general, the resistance decreases under applied pressure. A nonmonotonic change in the high-temperature resistance value for the $x = 0.12$ sample is possibly due to contact between the outside wiring and the piston cylinder pressure cell body in the first three pressure
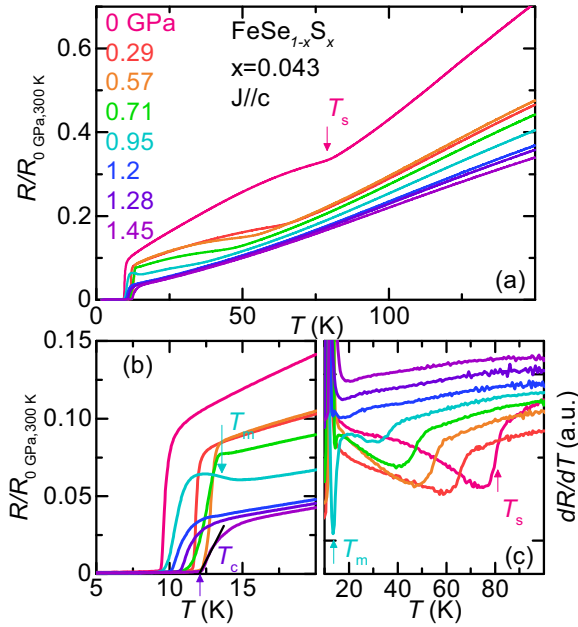
FIG. 3. (a) Evolution of the c-axis resistance with hydrostatic pressure for Fe(Se$_{1-x}$S$_x$), $x = 0.043$. Data were normalized at room temperature and ambient pressure. (b) Blowup of the low-temperature region. (c) Temperature derivative dR/dT showing the evolution of structural transition T_s. Examples of transition temperatures T_s, T_m, and T_c are indicated by arrows.

FIG. 4. (a) Evolution of the c-axis resistance with hydrostatic pressure for Fe(Se$_{1-x}$S$_x$), $x = 0.096$. Data were normalized at room temperature and ambient pressure. (b) Blowup of the low-temperature region. (c) Temperature derivative dR/dT showing the evolution of structural transition T_s.

runs. The kinklike anomaly, associated with the structural phase transition T_s, is clearly visible in the lower pressure data and appears as a steplike anomaly in the temperature derivative dR/dT [Figs. 2(c)–5(c)]. With increasing pressure, T_s is suppressed in all compounds. The blowup of the low-temperature region, presented in Figs. 2(b)–5(b), highlights nonmonotonic changes in T_c under increasing pressure. Furthermore, the superconducting transition broadens systematically under pressure, a tendency observed in the parent compound in the magnetically ordered phase. The increasing broadening of the superconducting transition under pressure could also be due to the inherent inhomogeneity of pressure when larger loads are applied, and the substituted samples may be increasingly sensitive to this inhomogeneity.

The magnified scale in Figs. 2(b)–5(b) reveals the effect of S substitution on T_m. For $x = 0.043$, an increase in resistance upon cooling is observed below 15 K for pressures between 0.71 and 1.03 GPa. This anomaly is reminiscent of the resistance increase at T_m of the parent compound at low pressures, shown in Fig. 2(b). We therefore associate it with the magnetic transition temperature T_m. In contrast to the parent compound, however, T_m is much less prominent in the S-substituted samples.

A magnetic field suppresses T_c but does not measurably affect T_m [15], allowing for the study of the magnetic transition in the absence of superconductivity. The application of a 9-T magnetic field, parallel to the c axis, permits us to discern T_m at pressures up to 1.28 GPa for the $x = 0.043$ sample (Fig. 6). An additional anomaly at temperatures slightly above T_m is observed for pressures greater than 0.95 GPa and is discussed in the Appendix.
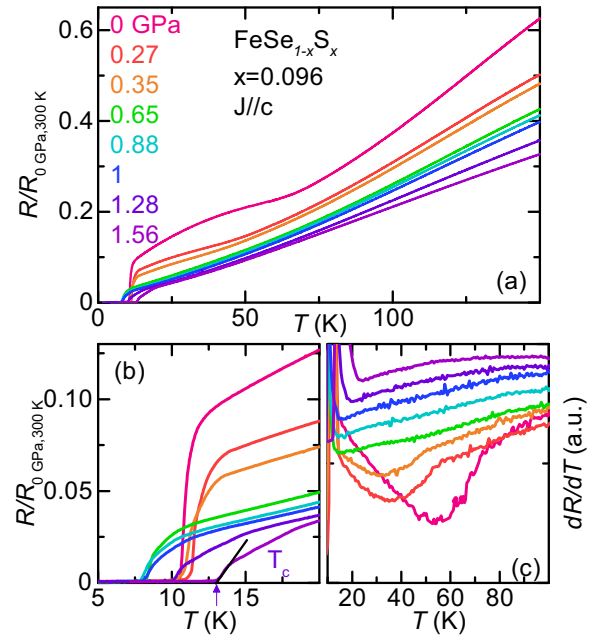
No feature corresponding to a possible magnetic transition is observed in the resistance data for $x = 0.096$ and $x = 0.12$ in zero magnetic field. However, the application of a 9-T magnetic field reveals a subtle resistance anomaly between 0.27 and 0.54 GPa for the $x = 0.096$ sample [Fig. 6(b)], which may be associated with T_m. For the $x = 0.12$ sample, even in a 9-T magnetic field, no anomaly that could be associated with magnetic ordering is observed in the resistance measurement with pressure up to 1.81 GPa. It is possible that the anomaly at T_m is less pronounced in the in-plane resistance, which was measured for the $x = 0.12$ sample and therefore was not resolved in these data.

The values of T_c, T_m, and T_s were obtained using the criteria outlined in Ref. [15] and shown in Figs. 2 and 3. T_c is defined as the intersection between the highest slope of $R(T)$ and zero resistance. T_s is defined as the midpoint of the step in dR/dT, i.e., the midpoint of the kink in $R(T)$, and T_m is defined as the point of the highest slope of the resistance. The resulting p-T phase diagrams of Fe(Se$_{1-x}$S$_x$), $x = 0$-0.12, are presented in Fig. 7.

The orthorhombic phase line is clearly resolved in all of the phase diagrams in the pressure range below $\sim$0.5$-$1.5 GPa. At ambient pressure, T_s is suppressed by 12% S substitution from 90 to 60 K. Pressure suppresses T_s almost linearly for all x but, as shown in Fig. 8(a), with an increased rate dT_s/dP for higher x.

For the parent compound FeSe, the magnetic transition at T_m was observed for pressures greater than 0.8 GPa [14,15]. Subsequent work showed the magnetic phase to persist up to 6 GPa, with a domelike dependence of T_m on pressure [16,17]. For the $x = 0.043$ sample, a similar phase line emerges above 0.5 GPa, and we tentatively associate it with T_m, pending
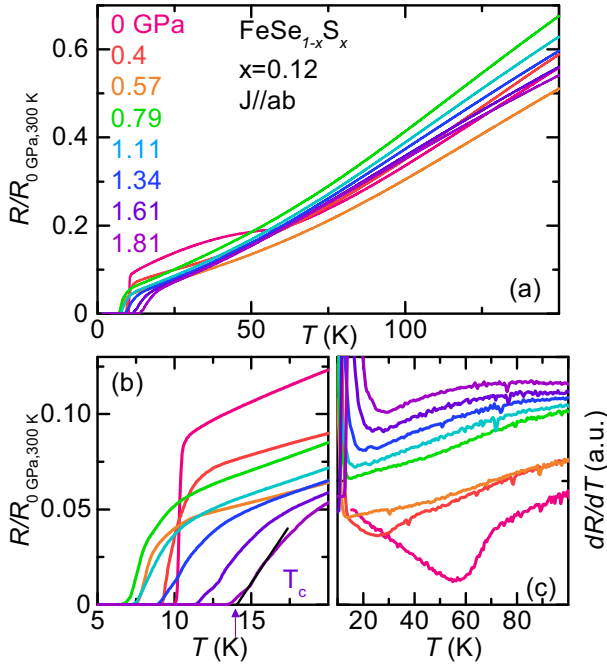
FIG. 5. (a) Evolution of the in-plane resistance with hydrostatic pressure for $\mathrm{Fe(Se_{1-x}S_x)}$, $x = 0.12$. Data were normalized at room temperature and ambient pressure. (b) Blowup of the low-temperature region. (c) Temperature derivative dR/dT showing the evolution of structural transition T_s.

confirmation by microscopic magnetic probes. But in contrast to pure FeSe, T_m increases only slightly to a maximum of 13.8 K at 0.71 GPa and is suppressed to below T_c already by 1.2 GPa. For higher S content, $x = 0.096$, this transition seems to occur within the small pressure range 0.27–0.57 GPa and with a domelike shape barely exceeding T_c at its maximum.
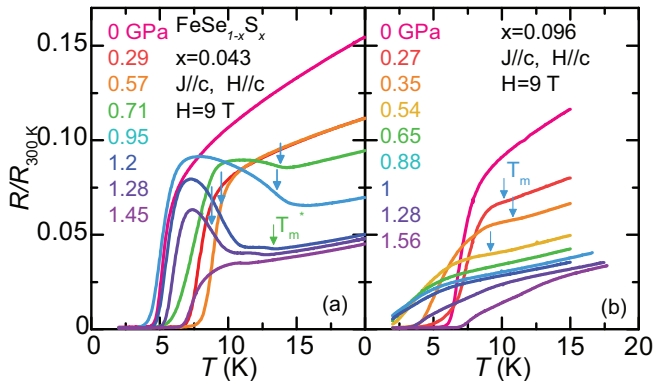

FIG. 6. Evolution of the temperature dependence of normalized resistance under various pressures with $H = 9$ T magnetic field applied parallel to c axis for (a) $x = 0.043$ and (b) $x = 0.096$. For the $x = 0.043$ sample, the magnetic phase transition indicated by blue arrows is more pronounced in field, and a second anomaly is observed at slightly higher temperatures. This anomaly, at T_m^*, is indicated by the green arrow and will be discussed in the Appendix. For $x = 0.096$, magnetic field reveals a subtle anomaly between 0.27 and 0.54 GPa, associated with the magnetic transition at T_m.
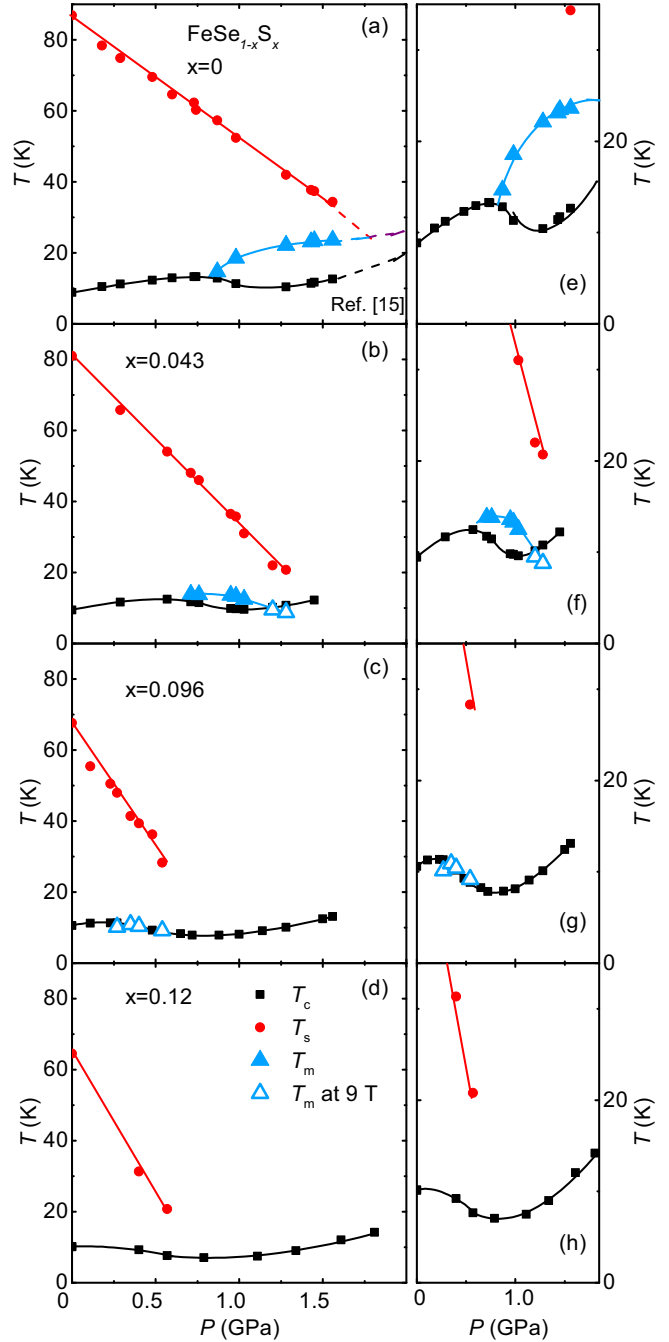

FIG. 7. Temperature-pressure phase diagrams of $\mathrm{Fe(Se_{1-x}S_x)}$ as determined from resistance measurements. The squares, circles, and triangles represent the superconducting T_c, structural T_s, and magnetic T_m phase transitions, respectively. The solid lines are guides to the eye. Data in (a) and (e) are taken from Ref. [15]. The dashed lines in (a) represent extrapolations based of Refs. [14,18]. As shown in (a)–(d), for all compounds T_s is suppressed linearly with increasing pressure. (e)–(h) show the data on an expanded temperature scale. T_c shows similar nonmonotonic dependence on pressure with a local maximum and minimum. The magnetic order appears strongly suppressed upon substitution. The intersection of the T_s lines and T_c lines is not unique and does not coincide universally with either the minimum or the maximum of T_c.
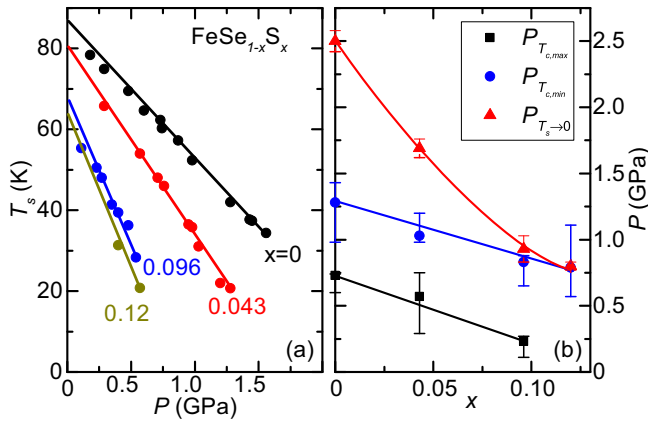
FIG. 8. (a) Pressure dependence of the structural transition temperature T_s for $Fe(Se_{1-x}S_x)$ with different substitution levels x. (b) Substitution dependence of the pressures $P_{Tc,max}$, $P_{Tc,min}$, and $P_{T_s \to 0}$, which correspond to the local maximum of T_c, minimum of T_c, and the extrapolation of T_s to zero temperature, respectively. Solid lines are guides to the eyes. Data for $x = 0$ are taken from Ref. [15].

For $x = 0.12$, no corresponding transition is resolved in the in-plane resistance measurement.

For all measured substitution levels, T_c of $Fe(Se_{1-x}S_x)$ shows a similar nonmonotonic dependence on pressure. The local maximum of T_c shifts to lower pressure on increasing sulfur content, from $P_{Tc,max} = 0.73$ GPa for $x = 0$ to 0.23 GPa for $x = 0.096$ and close to ambient pressure for $x = 0.12$. Likewise, the local minimum of T_c shifts from $P_{Tc,min} = 1.28$ GPa for $x = 0$ to 0.79 GPa for $x = 0.12$, as presented in Fig. 8(b).

The clear suppression of T_c below its local maximum in the intermediate pressure range is similar for all studied substitution levels. The onset of this suppression correlates with the emergence of the magnetic phase for $x = 0$–0.096, even though in the $x = 0.096$ sample, T_m is indicated only by an extremely weak feature in resistivity and practically coincides with T_c. For $x = 0.12$, T_m is not visible at all. It seems likely that the competing order setting in at T_m suppresses T_c for $x = 0$–0.096. However, whether this is still the case at higher substitution levels remains an open question, and possibly another mechanism for the partial suppression of T_c needs to be invoked.

The minimum of T_c of pure FeSe at 1.3 GPa likely coincides with a change in the Fermi-surface under pressure [15,37]. It is plausible that a similar change in the Fermi surface occurs in the doped samples and is the origin of the local minimum of T_c. In contrast, the extrapolations of the T_s phase lines intersect T_c at nonunique positions for the different substitution levels. The extrapolation does not correlate universally with either the maximum or the minimum of T_c in $Fe(Se_{1-x}S_x)$, $x = 0$–0.12 [Fig. 8(b)]. This behavior differs from many other iron-based superconductor phase diagrams, where T_s and T_c typically intersect near the maximum of T_c [2].

$Fe(Se_{0.904}S_{0.096})$ provides an example in which the structural transition extrapolates to the minimum of T_c. Several theories have discussed the influence of a nematic phase, in particular a nematic quantum critical point, on superconductivity [38,39]. In all cases, the nematic fluctuations are assumed

to enhance (or induce) superconducting pairing and correlate with a maximum in T_c, opposite the observed behavior. This is a sign that nematic fluctuations may not be involved in the superconducting pairing in this compound.

The magnetic phase in the low-pressure range is extremely sensitive to S substitution, but the orthorhombic/nematic phase is not. For example, in $Fe(Se_{0.957}S_{0.043})$ we observe only a tiny magnetic dome, contained entirely inside the nematic phase. In pure FeSe, T_m increases under applied pressure until T_s and T_m merge. The increase of orthorhombic distortion below T_m in FeSe demonstrates the cooperative coupling of the two types of order [18], similar to many iron-arsenide materials [35]. In the well-known spin-nematic scenario for iron-arsenide materials [40], the nematic transition is believed to be a consequence of incipient stripe-type magnetic order. The strikingly different responses of nematic and magnetic order to sulfur substitution in FeSe suggest, however, that the nematic phase in $Fe(Se_{1-x}S_x)$ may not be related to the magnetic order observed in the low-pressure range. A number of alternative scenarios for the origin of nematic order in FeSe have been put forward, including quadrupolar order [20,21], frustrated quantum paramagnetism [41], and a Pomeranchuk instability [22].

Isovalent substitution, as the replacement of selenium by sulfur, may be thought of as chemical pressure. Well-known examples in the iron-arsenide systems are $BaFe_2(As_{1-x}P_x)_2$ and $Ba(Fe_{1-x}Ru_x)_2As_2$ [42–45]. If pressure and substitution were simply additive, the p-T phase diagrams for different substitution levels would be shifted with respect to each other. This is clearly not the case for the transition at T_m in $Fe(Se_{1-x}S_x)$, whose maximum temperature is strongly suppressed with increasing x. Sulfur substitution and pressure are not additive concerning T_s either. Figure 8(a) shows the T_s phase lines for the four substitution levels, $x = 0$, 0.043, 0.096, and 0.12. Both substitution and pressure suppress T_s, but the rate of suppression of T_s under pressure depends on the substitution level. This would not be the case if S substitution was simply additive to pressure. Similarly, an overlap of the S-shaped pressure dependence of T_c for different x cannot be achieved by a simple shift. Even though $P_{Tc,max}$ and $P_{Tc,min}$ are suppressed at a similar rate by sulfur substitution [Fig. 8(b)], this S changes shape for increasing sulfur content. These comparisons demonstrate that sulfur substitution and physical pressure are not equivalent in FeSe concerning any phase transition and likely modify the electronic structure as well as any salient coupling constants in different ways.

IV. PRESSURE DEPENDENCE OF THE UPPER CRITICAL FIELD

To better understand the superconducting properties of $Fe(Se_{1-x}S_x)$, including the nonmonotonic pressure dependence of T_c, the superconducting upper critical field is analyzed following Refs. [15,46]. Figures 9, 10, and 11 show the temperature dependence of the upper critical field H_{c2} for $H||c$ of $Fe(Se_{1-x}S_x)$ for $x = 0.043$, $x = 0.096$, and $x = 0.12$ at various pressures. The insets show the temperature dependence of resistance in magnetic fields $H \parallel c$ between 0 and 9 T, from which these data are obtained, for representative pressure values. Notably, for the $x = 0.12$ sample, the current was
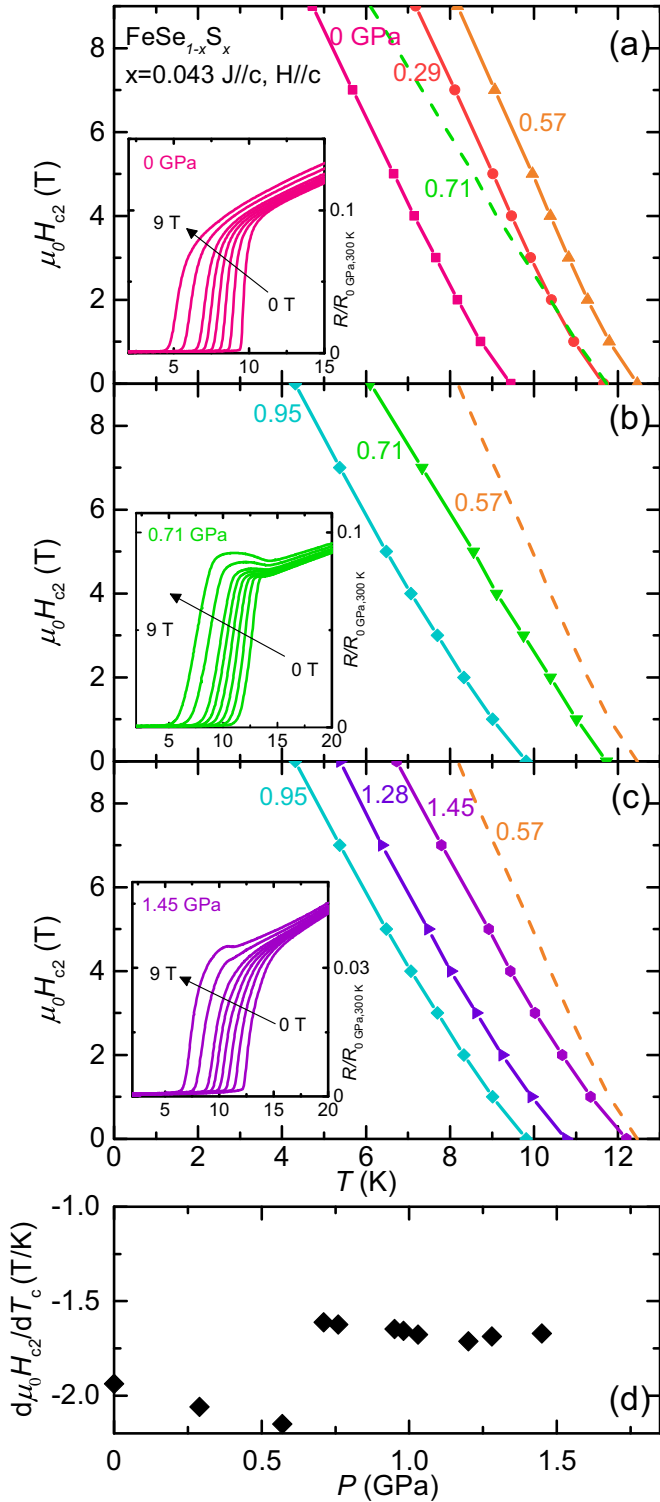
FIG. 9. Temperature dependence of the upper critical field $H_{c2}(T)$ measured in the $j \parallel H \parallel c$ configuration under various pressures for the $x = 0.043$ sample. (a)–(c) Three regions are identified and separated by the local maximum and minimum of T_c under pressure. (d) A clear change in the $H_{c2}(T)$ slope is observed between only the first and second regions. Insets show representative resistance data under magnetic fields up to 9 T.
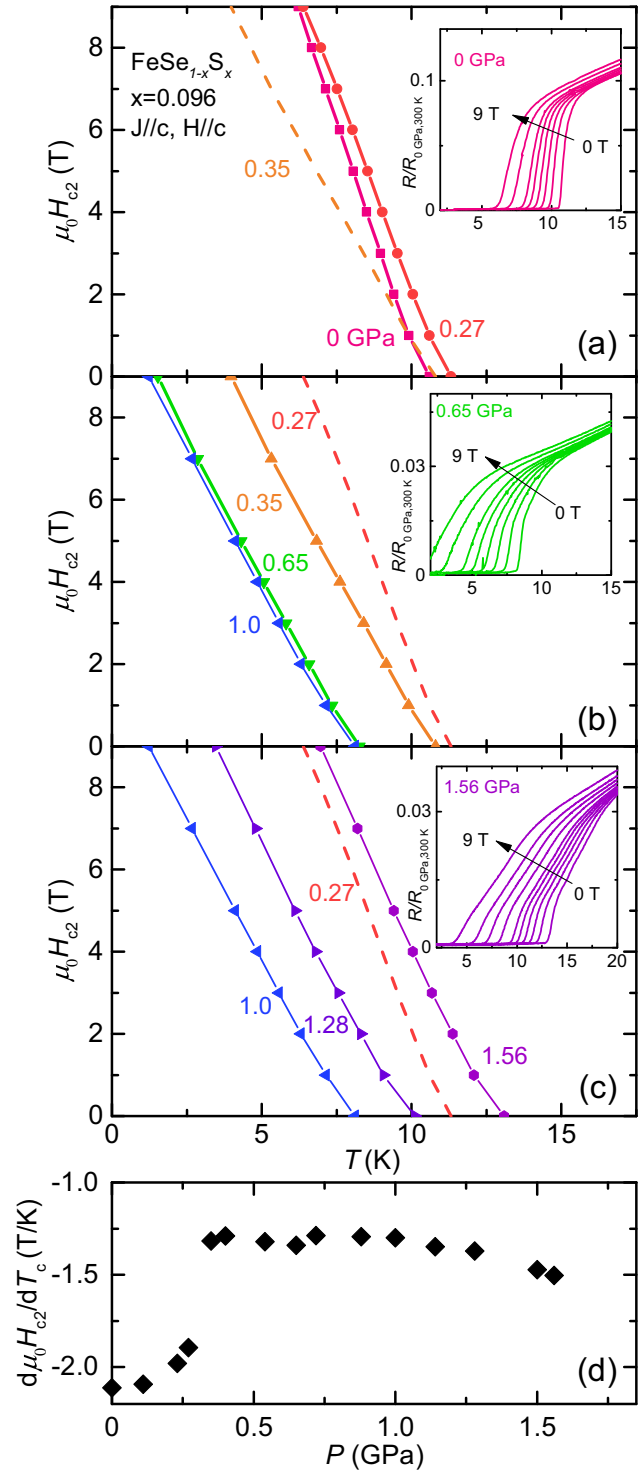
FIG. 10. Temperature dependence of the upper critical field $H_{c2}(T)$ measured in the $j \parallel H \parallel c$ configuration under various pressures for the $x = 0.096$ sample. (a)–(c) Three regions are identified and separated by the local maximum and minimum of T_c under pressure. (d) A clear change in the $H_{c2}(T)$ slope is observed between only the first and second regions. Insets show representative resistance data under magnetic fields up to 9 T.
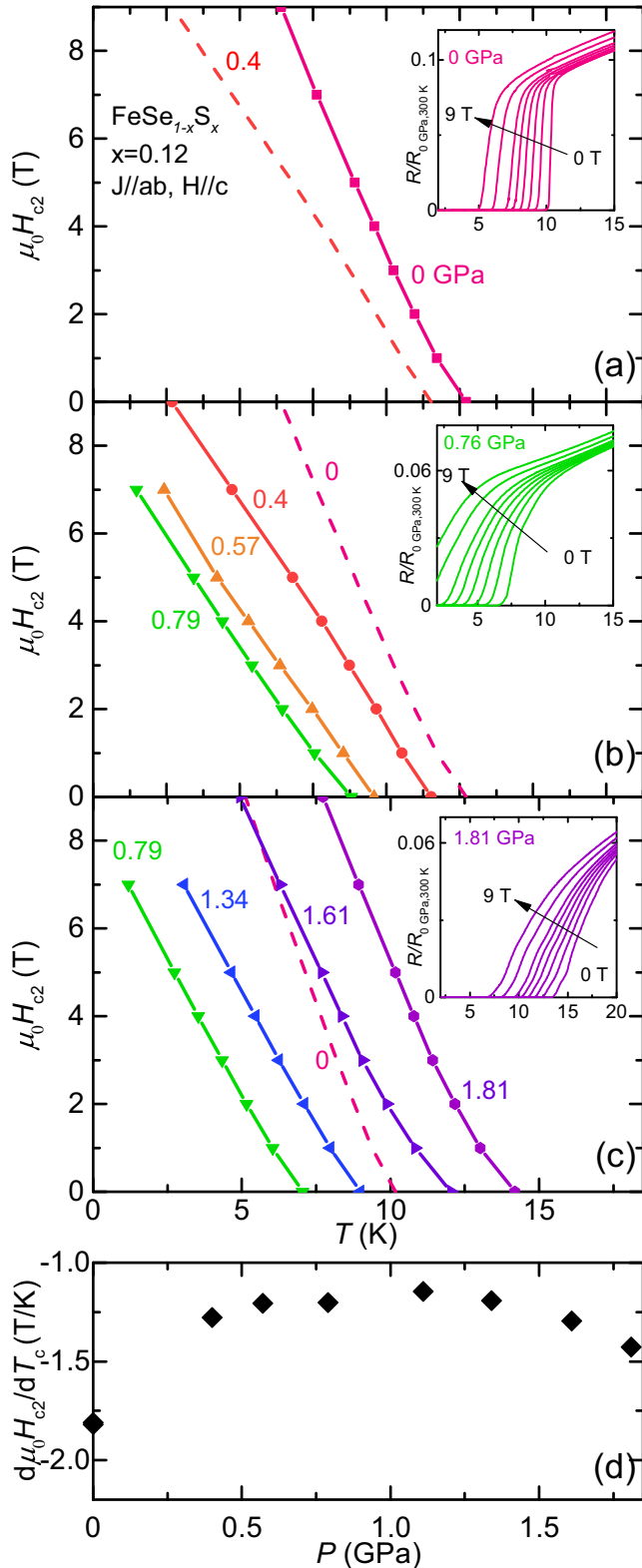
FIG. 11. Temperature dependence of the upper critical field $H_{c2}(T)$ measured in the $H \parallel c$, $j \parallel ab$ configuration under various pressures for the $x = 0.12$ sample. (a)–(c) Three regions are identified and separated by the local maximum and minimum of T_c under pressure. (d) A clear change in the $H_{c2}(T)$ slope is observed between only the first and second regions. Insets show representative resistance data under magnetic fields up to 9 T.

applied along the ab plane, whereas the current was along the c axis for the other compounds. In principle, the $j \parallel H \parallel c$ configuration can minimize the contribution of flux flow to the superconducting transitions, but no fundamental difference with different current directions was observed between the measurements. At ambient pressure, the superconducting transition remains sharp for all field values. As the pressure is increased, the superconducting transition becomes broader, especially in the $x = 0.096$ and $x = 0.12$ samples.

A distinct change in the slope of $H_{c2}(T)$, which is obtained by fitting the 0–9-T data, is observed between 0.57 and 0.71 GPa for $x = 0.043$, and between 0.27 and 0.35 GPa for $x = 0.096$. For $x = 0.12$, a slope change occurs between ambient pressure and 0.4 GPa [Figs. 9(d)–11(d)]. These pressure ranges are close to the local maximum of T_c and, for $x = 0.043$ and $x = 0.096$, the onset of magnetic order. No abrupt slope change of H_{c2} occurs around the pressure-associated local minimum of T_c.

Figure 12 shows the pressure evolution of the upper critical field slope normalized by T_c, $-[d\mu_0 H_{c2}/dT_c]/T_c$, and of the transition temperatures T_c, T_s, and T_m for $x = 0$ [15], $x = 0.043$, $x = 0.096$, and $x = 0.12$. For all substitution levels, $-[d\mu_0 H_{c2}/dT_c]/T_c$ exhibits a sudden decrease near the local maximum of T_c under pressure. For the substituted compounds, a more continuous change is observed near the local minimum of T_c, at which point $-[d\mu_0 H_{c2}/dT_c]/T_c$ has a broad maximum.

Generally speaking, the slope of the upper critical field normalized by T_c is related to the Fermi velocity and superconducting gap of the system [47]. In the clean limit for a single-band case,

$$-[d\mu_o H_{c2}/dT_c]/T_c \propto 1/v_F^2, \tag{1}$$

where v_F is the Fermi velocity. Note that the mass enhancement expected at a quantum critical point should result in an increase of $-[d\mu_o H_{c2}/dT_c]/T_c$ [5]. The superconducting gap structure and, in a multiband case, the coupling constants for the different bands are also involved [47]. A change in the normalized slope of H_{c2} may result from changes in the Fermi surface, the superconducting gap structure, or the pairing mechanism [46,47]. In addition, a change in scattering rates can also change H_{c2} [48]. It was previously shown in pure FeSe that both the decrease of $-[d\mu_o H_{c2}/dT_c]/T_c$ close to the local maximum of T_c and its increase close to the local minimum of T_c under pressure can be explained by changes in the Fermi velocity [15].

Similar to pure FeSe, $-[d\mu_o H_{c2}/dT_c]/T_c$ of Fe(Se$_{1-x}$S$_x$) displays an abrupt decrease close to the local maximum of T_c under pressure for all studied substitution levels. This points to a change in the Fermi velocity similar to that in the parent compound and supports the identification of this pressure level with the emergence of magnetic order, entailing a reconstruction of the Fermi surface. Possibly, a change in electronic scattering rates at the onset of magnetic order also influences H_{c2}. The subsequent broad maximum of $-[d\mu_o H_{c2}/dT_c]/T_c$ results from dividing an almost-pressure-independent $d\mu_o H_{c2}/dT_c$ [Figs 9(d)–11(d)] by T_c since T_c displays a minimum in this pressure range. This maximum of the normalized slope of H_{c2} may also be associated with a
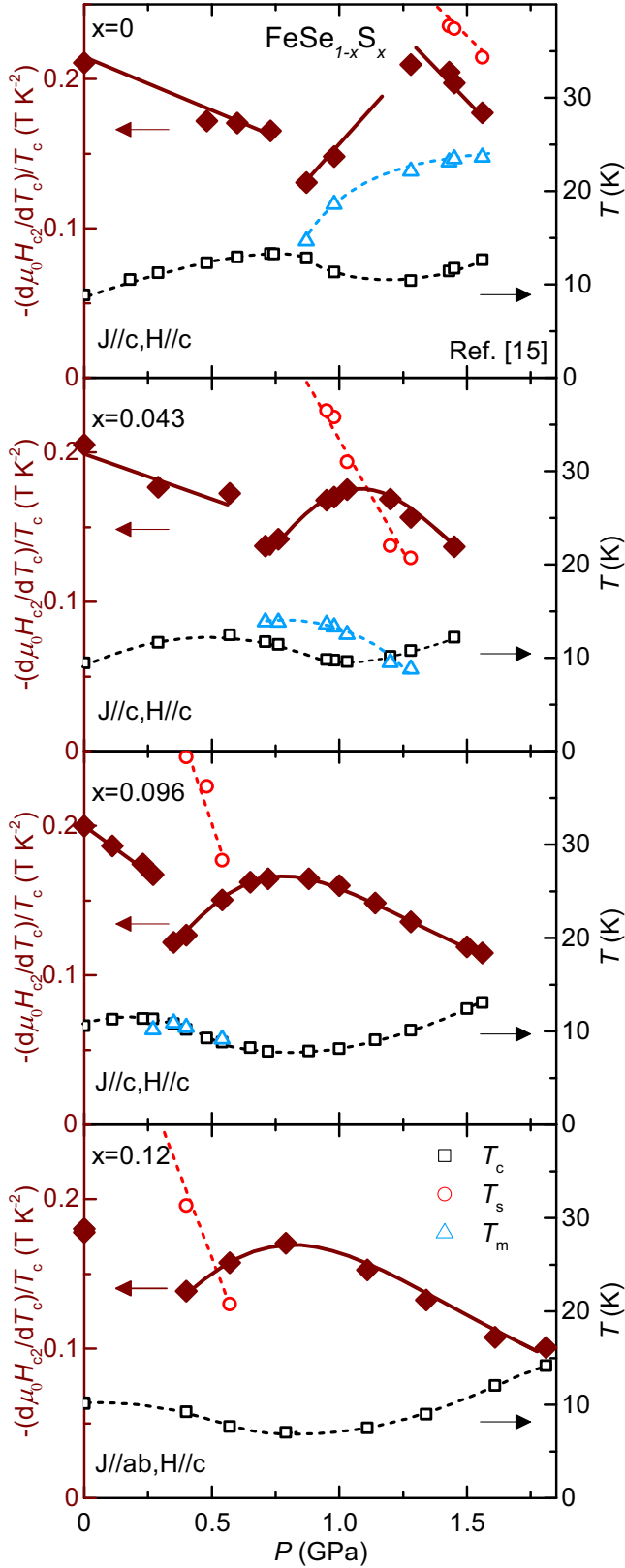
FIG. 12. Pressure dependence of the normalized upper critical field slope $-[d\mu_o H_{c2}/dT_c]/T_c$, plotted together with T_c, T_s, and T_m. For all compounds, an abrupt change in the slope is observed near the local maximum of T_c. For the sulfur-containing compounds, a more continuous change in the slope occurs near the local minimum of T_c. Data in the top panel are taken from Ref. [15].
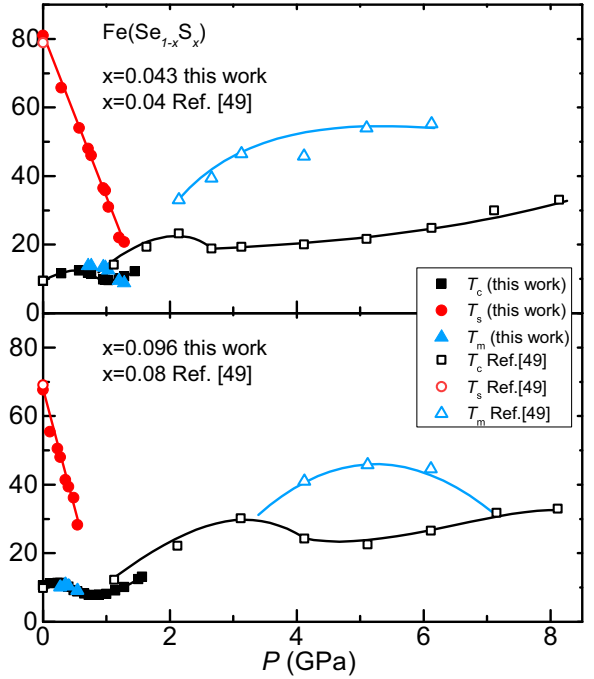

FIG. 13. Temperature-pressure phase diagrams of Fe(Se$_{1-x}$S$_x$) up to 8 GPa, including data from Ref. [49]. The squares, circles, and triangles represent the superconducting T_c, structural T_s, and magnetic T_m phase transitions, respectively. Data from samples with similar T_s values at ambient pressure are combined. The solid lines are guides to the eye. This represents an extension of our detailed low-pressure phase diagrams presented in Fig. 7.

pressure-induced Fermi surface change or with a gradual mass enhancement at this pressure. Note that a pressure-independent $d\mu_o H_{c2}/dT_c$ indicates that $T_c \propto v_F^2$, according to Eq. (1).

V. CONCLUSION

In conclusion, the temperature-dependent resistance of sulfur-substituted FeSe$_{1-x}$S$_x$ ($x = 0.043, 0.096, 0.12$) has been studied under pressures up to 1.8 GPa and in magnetic fields up to 9 T. T_c exhibits a similar, nonmonotonic pressure dependence with a local maximum and a local minimum for all substitution levels. T_s is suppressed by pressure, at increasing rates for higher sulfur contents. The magnetic phase in the low-pressure range is strongly suppressed by substitution, which raises the question of how closely magnetic order and orthorhombic phase are related. Abrupt changes in the normalized slope of the upper critical field $-[d\mu_o H_{c2}/dT_c]/T_c$ near the local maximum of T_c may indicate a Fermi-surface reconstruction coinciding with the transition at T_m for $x = 0$–0.096 and suggest its existence in $x = 0.12$ as well. Another change in the Fermi surface likely occurs near the local minimum of T_c at slightly higher pressures. These results highlight the differences between chemical pressure and physical pressure as tuning parameters for FeSe.

Note added. Recently, related results on the pressure-temperature phase diagrams of Fe(Se$_{1-x}$S$_x$) ($x = 0.04$–0.17) with a focus on the higher-pressure range 2–8 GPa were made available [49]. By means of resistivity measurements in a cubic anvil cell, a prominent dome of likely magnetic order was

found to exist in the higher-pressure range, detached from the nematic phase for $x \geqslant 0.04$. Taken together with the results presented here, this indicates that the pressure-temperature phase diagram of lightly S substituted $Fe(Se_{1-x}S_x)$ features two magnetic phases (see Fig. 13), possibly resulting from a splitting of the single pressure-induced magnetic dome of pure FeSe. The mechanism by which such a splitting would occur remains to be studied, as, indeed, does the microscopic nature of the pressure-induced phases and their relation to each other. Altogether, the recent results reveal the astounding complexity of pressure- and substitution-tuned FeSe.

APPENDIX

Figure 14 presents the low-temperature resistance data for $FeSe_{0.904}S_{0.096}$ in the pressure range 0.27–0.54 GPa and under applied magnetic fields up to 9 T. The superconductivity is suppressed by the applied magnetic field. For fields greater than 7 T, a slight upturn of the resistance is observed. We associate this anomaly with magnetic phase transition, and the corresponding T_m at 9 T is indicated by an arrow.

An additional anomaly is observed in the resistance measurement for $FeSe_{0.957}S_{0.043}$ under pressure. As shown in Fig. 15, in the pressure range 0.95–1.45 GPa, two anomalies emerge above the superconducting transition. We associate the lower-temperature anomaly with the magnetic transition T_m due to its similarities with the parent compound FeSe
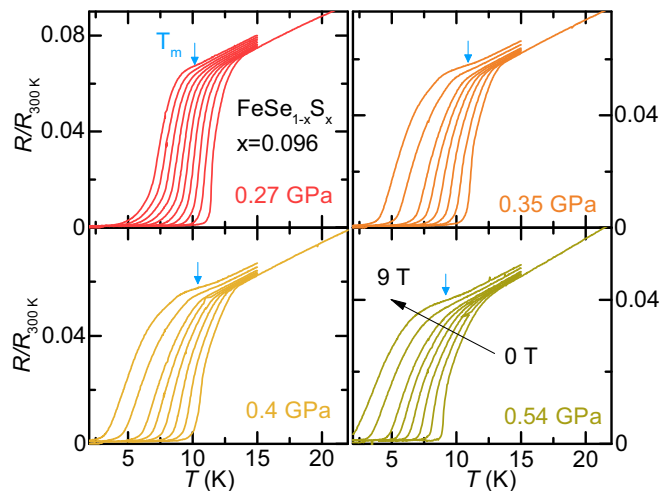

FIG. 15. Temperature dependence of the normalized resistance under magnetic field up to 9 T for selected pressures for the compound $FeSe_{1-x}S_x$, $x = 0.043$. Two anomalies associated with magnetic transition T_m and possibly another magnetic transition T_m^* are indicated by arrows.

[16]. The other anomaly, labeled T_m^*, occurs slightly above T_m and is indicated in Figs. 6 and 15. For 0.71 GPa, only T_m is observed. From 0.95 to 1.03 GPa, both of these anomalies can be seen in zero-field-resistance measurements. Furthermore, with application of magnetic fields up to 9 T, these two anomalies barely shift. At higher
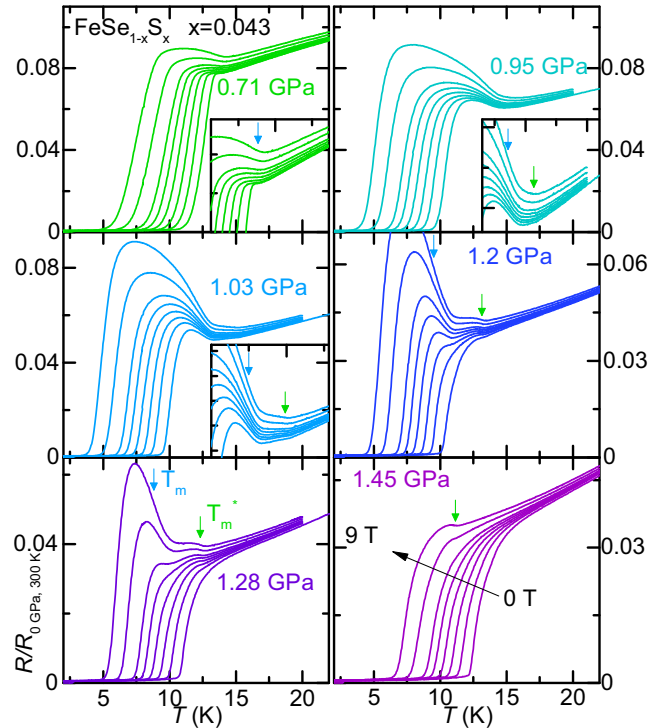

FIG. 14. Temperature dependence of the normalized resistance under magnetic field up to 9 T for selected pressures for the compound $FeSe_{1-x}S_x$, $x = 0.096$. The anomaly associated with magnetic transition T_m is indicated by an arrow.
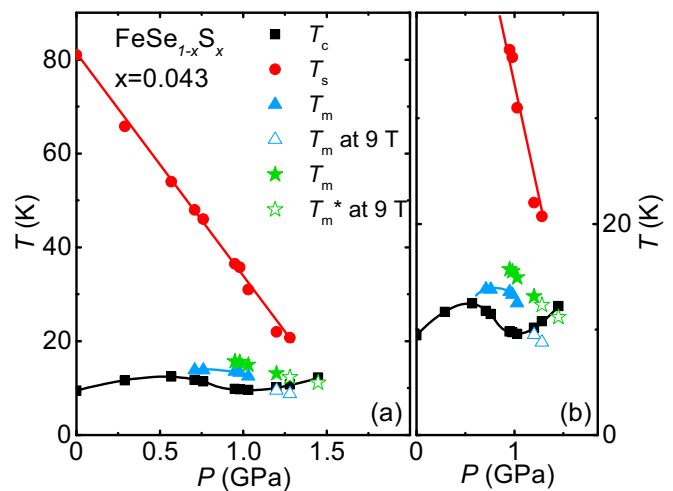

FIG. 16. Extended temperature-pressure phase diagram of $FeSe_{0.957}S_{0.043}$ as determined from resistance measurement as in Fig. 7. T_m^*, indicated by green stars, represents the new anomaly we observed in this compound. The solid lines are guides for the eye.

pressures, 1.2–1.45 GPa, those anomalies are no longer discernible in the zero-field-resistance measurements. However, by suppressing the superconducting transition with magnetic field, they are revealed in resistance for 1.2 and 1.28 GPa. At our highest pressure of 1.45 GPa, only T_m^* could be observed.

The temperature-pressure phase diagram of $FeSe_{0.957}S_{0.043}$ complemented by including T_m^* is presented in Fig. 16. T_m exhibits a domelike pressure dependence, whereas T_m^* emerges on the high-pressure side of this dome. Whether this new anomaly T_m^* is related to a possible incommensurate magnetic transition or a different phase transition needs further study.

[1] P. C. Canfield and S. L. Bud'ko, Annu. Rev. Condens. Matter Phys. **1**, 27 (2010).

[2] J. Paglione and R. L. Greene, Nat. Phys. **6**, 645 (2010).

[3] R. M. Fernandes, A. V. Chubukov, and J. Schmalian, Nat. Phys. **10**, 97 (2014).

[4] S. Kasahara, T. Shibauchi, K. Hashimoto, K. Ikada, S. Tonegawa, R. Okazaki, H. Shishido, H. Ikeda, H. Takeya, K. Hirata, T. Terashima, and Y. Matsuda, Phys. Rev. B **81**, 184519 (2010).

[5] C. Putzke, P. Walmsley, J. D. Fletcher, L. Malone, D. Vignolles, C. Proust, S. Badoux, P. See, H. E. Beere, D. A. Ritchie, S. Kasahara, Y. Mizukami, T. Shibauchi, Y. Matsuda, and A. Carrington, Nat. Commun. **5**, 5679 (2014).

[6] T. M. McQueen, A. J. Williams, P. W. Stephens, J. Tao, Y. Zhu, V. Ksenofontov, F. Casper, C. Felser, and R. J. Cava, Phys. Rev. Lett. **103**, 057002 (2009).

[7] S.-H. Baek, D. V. Efremov, J. M. Ok, J. S. Kim, J. van den Brink, and B. Büchner, Nat. Mater. **14**, 210 (2014).

[8] A. E. Böhmer, T. Arai, F. Hardy, T. Hattori, T. Iye, T. Wolf, H. v. Löhneysen, K. Ishida, and C. Meingast, Phys. Rev. Lett. **114**, 027001 (2015).

[9] M. D. Watson, T. K. Kim, A. A. Haghighirad, N. R. Davies, A. McCollam, A. Narayanan, S. F. Blake, Y. L. Chen, S. Ghannadzadeh, A. J. Schofield, M. Hoesch, C. Meingast, T. Wolf, and A. I. Coldea, Phys. Rev. B **91**, 155106 (2015).

[10] M. Bendele, A. Amato, K. Conder, M. Elender, H. Keller, H.-H. Klauss, H. Luetkens, E. Pomjakushina, A. Raselli, and R. Khasanov, Phys. Rev. Lett. **104**, 087003 (2010).

[11] G. Chen, X. Zhu, H. Yang, and H. Wen, arXiv:1703.08680.

[12] J.-Y. Lin, Y. S. Hsieh, D. A. Chareev, A. N. Vasiliev, Y. Parsons, and H. D. Yang, Phys. Rev. B **84**, 220507 (2011).

[13] M. Bendele, A. Ichsanow, Y. Pashkevich, L. Keller, T. Strässle, A. Gusev, E. Pomjakushina, K. Conder, R. Khasanov, and H. Keller, Phys. Rev. B **85**, 064517 (2012).

[14] T. Terashima, N. Kikugawa, S. Kasahara, T. Watashige, T. Shibauchi, Y. Matsuda, T. Wolf, A. E. Böhmer, F. Hardy, C. Meingast, H. v. Löhneysen, and S. Uji, J. Phys. Soc. Jpn. **84**, 063701 (2015).

[15] U. S. Kaluarachchi, V. Taufour, A. E. Böhmer, M. A. Tanatar, S. L. Bud'ko, V. G. Kogan, R. Prozorov, and P. C. Canfield, Phys. Rev. B **93**, 064503 (2016).

[16] J. P. Sun, K. Matsuura, G. Z. Ye, Y. Mizukami, M. Shimozawa, K. Matsubayashi, M. Yamashita, T. Watashige, S. Kasahara, Y. Matsuda, J. Q. Yan, B. C. Sales, Y. Uwatoko, J. G. Cheng, and T. Shibauchi, Nat. Commun. **7**, 12146 (2016).

[17] J. P. Sun, G. Z. Ye, P. Shahi, J.-Q. Yan, K. Matsuura, H. Kontani, G. M. Zhang, Q. Zhou, B. C. Sales, T. Shibauchi, Y. Uwatoko, D. J. Singh, and J.-G. Cheng, Phys. Rev. Lett. **118**, 147004 (2017).

[18] K. Kothapalli, A. E. Böhmer, W. T. Jayasekara, B. G. Ueland, P. Das, A. Sapkota, V. Taufour, Y. Xiao, E. Alp, S. L. Bud'ko, P. C. Canfield, A. Kreyssig, and A. I. Goldman, Nat. Commun. **7**, 12728 (2016).

[19] J. K. Glasbrenner, I. I. Mazin, H. O. Jeschke, P. J. Hirschfeld, R. M. Fernandes, and R. Valenti, Nat. Phys. **11**, 953 (2015).

[20] R. Yu and Q. Si, Phys. Rev. Lett. **115**, 116401 (2015).

[21] Z. Wang, W.-J. Hu, and A. H. Nevidomskyy, Phys. Rev. Lett. **116**, 247203 (2016).

[22] A. V. Chubukov, M. Khodas, and R. M. Fernandes, Phys. Rev. X **6**, 041045 (2016).

[23] K. Miyoshi, J. Phys. Soc. Jpn. **83**, 013702 (2014).

[24] J.-F. Ge, Z.-L. Liu, C. Liu, C.-L. Gao, D. Qian, Q.-K. Xue, Y. Liu, and J.-F. Jia, Nat. Mater. **14**, 285 (2015).

[25] Y. Mizuguchi, F. Tomioka, S. Tsuda, T. Yamaguchi, and Y. Takano, J. Phys. Soc. Jpn. **78**, 074712 (2009).

[26] M. D. Watson, T. K. Kim, A. A. Haghighirad, S. F. Blake, N. R. Davies, M. Hoesch, T. Wolf, and A. I. Coldea, Phys. Rev. B **92**, 121108 (2015).

[27] A. I. Coldea, S. F. Blake, S. Kasahara, A. A. Haghighirad, M. D. Watson, W. Knafo, E. S. Choi, A. McCollam, P. Reiss, T. Yamashita, M. Bruma, S. Speller, Y. Matsuda, T. Wolf, T. Shibauchi, and A. J. Schofield, arXiv:1611.07424.

[28] S. Hosoi, K. Matsuura, K. Ishida, H. Wang, Y. Mizukami, T. Watashige, S. Kasahara, Y. Matsuda, and T. Shibauchi, Proc. Natl. Acad. Sci. USA **113**, 8139 (2016).

[29] Y. A. Ovchenkov, D. A. Chareev, D. E. Presnov, O. S. Volkova, and A. N. Vasiliev, J. Low Temp. Phys. **185**, 467 (2016).

[30] A. E. Böhmer, V. Taufour, W. E. Straszheim, T. Wolf, and P. C. Canfield, Phys. Rev. B **94**, 024526 (2016).

[31] M. A. Tanatar, N. Ni, G. D. Samolyuk, S. L. Bud'ko, P. C. Canfield, and R. Prozorov, Phys. Rev. B **79**, 134528 (2009).

[32] M. A. Tanatar, A. E. Böhmer, E. I. Timmons, M. Schütt, G. Drachuck, V. Taufour, K. Kothapalli, A. Kreyssig, S. L. Bud'ko, P. C. Canfield, R. M. Fernandes, and R. Prozorov, Phys. Rev. Lett. **117**, 127001 (2016).

[33] S. Bud'ko, A. Voronovskii, A. Gapotchenko, and E. ltskevich, Zh. Eksp. Teor. Fiz. **86**, 778 (1984) [Sov. Phys. JETP **59**, 454 (1984)].

[34] B. Bireckoven and J. Wittig, J. Phys. E: Sci. Instrum. **21**, 841 (1988).

[35] S. K. Kim, M. S. Torikachvili, E. Colombier, A. Thaler, S. L. Bud'ko, and P. C. Canfield, Phys. Rev. B **84**, 134525 (2011).

[36] M. S. Torikachvili, S. K. Kim, E. Colombier, S. L. Bud'ko, and P. C. Canfield, Rev. Sci. Instrum. **86**, 123904 (2015).

[37] T. Terashima, N. Kikugawa, A. Kiswandhi, D. Graf, E.-S. Choi, J. S. Brooks, S. Kasahara, T. Watashige, Y. Matsuda, T. Shibauchi, T. Wolf, A. E. Böhmer, F. Hardy, C. Meingast, H. v. Löhneysen, and S. Uji, Phys. Rev. B **93**, 094505 (2016).

[38] S. Lederer, Y. Schattner, E. Berg, and S. A. Kivelson, Phys. Rev. Lett. **114**, 097001 (2015).

[39] D. Labat and I. Paul, arXiv:1703.04146.

[40] R. M. Fernandes and J. Schmalian, Supercond. Sci. Technol. **25**, 084005 (2012).

[41] F. Wang, S. A. Kivelson, and D.-H. Lee, Nat. Phys. **11**, 959 (2015).

[42] L. E. Klintberg, S. K. Goh, S. Kasahara, Y. Nakai, K. Ishida, M. Sutherland, T. Shibauchi, Y. Matsuda, and T. Terashima, J. Phys. Soc. Jpn. **79**, 123706 (2010).

[43] S. Jiang, H. Xing, G. Xuan, C. Wang, Z. Ren, C. Feng, J. Dai, Z. Xu, and G. Cao, J. Phys. Condens. Matter **21**, 382203 (2009).

[44] E. Colombier, S. L. Bud'ko, N. Ni, and P. C. Canfield, Phys. Rev. B **79**, 224518 (2009).

[45] A. Thaler, N. Ni, A. Kracher, J. Q. Yan, S. L. Bud'ko, and P. C. Canfield, Phys. Rev. B **82**, 014534 (2010).

[46] V. Taufour, N. Foroozani, M. A. Tanatar, J. Lim, U. Kalu-arachchi, S. K. Kim, Y. Liu, T. A. Lograsso, V. G. Kogan, R. Prozorov, S. L. Bud'ko, J. S. Schilling, and P. C. Canfield, Phys. Rev. B **89**, 220509 (2014).

[47] V. G. Kogan and R. Prozorov, Rep. Prog. Phys. **75**, 114502 (2012).

[48] V. G. Kogan and R. Prozorov, Phys. Rev. B **90**, 180502 (2014).

[49] K. Matsuura, Y. Mizukami, Y. Arai, Y. Sugimura, N. Maejima, A. Machida, T. Watanuki, T. Fukuda, T. Yajima, Z. Hiroi, K. Y. Yip, Y. C. Chan, Q. Niu, S. Hosoi, K. Ishida, K. Mukasa, T. Watashige, S. Kasahara, J.-G. Cheng, S. K. Goh, Y. Matsuda, Y. Uwatoko, and T. Shibauchi, arXiv:1704.02057.